Effect of Carbon and Titanium Addition on Erosive Wear Behavior of High Chromium White Cast Irons

Technical Paper

Effect of Carbon and Titanium Addition on Erosive Wear Behavior of High Chromium White Cast Irons

Mohammad Jobayer Huq [1], Kazumichi Shimizu[1], Kenta Kusumoto[1,*], Riki Hendra Purba[1] and Yila Gaqi[1]

Muroran Institute of Technology, 27-1 Mizumoto, Muroran City 050-8585, Japan

* Correspondence: kusumoto@mmm.muroran-it.ac.jp

Abstract

The damage due to wear is rigorous both financially and environmentally.Developing a wear resistant material is the prerequisite to reduce cost due to wear related damage and ensure a green environment. High chromium white cast iron (HCCI) is highly valuated owing to its prominent wear resistance behaviour.The combined effect of added Ti and C with HCCI to tackle the erosive wear is investigated in this paper. Ti and C are supplemented in variable percentages. TiC precipitation happens due to Ti addition while M_7C_3 experience noticable refinement in the matrix. The TiC crystallization results to shortage of C in the matrix and M_7C_3 refinement leads to lower hardness. The enhancement in the percentage of added Ti deteriorates the hardness causes to foster the wear rate. On the contrary, the increase in carbon content advances the hardness which reduces the wear rate. It is believed that the previously consumed C by Ti weekens the matrix. However, increment in C strengthen it with coarse carbide M_7C_3.Among the three series of test specimens with 3wt%,3.5wt%, and 4wt%C contents.Greater hardness is observed in 4wt%C contributes to highest wear resistance . This study figured out that the chemical composition of minimal Ti and maximum C with HCCI can resist the erosive wear substantially.

Keywords: Erosive wear; High chromium white cast iron; Titanium; Carbon

Introduction

Erosive wear or erosion is a surface damage phenomenon that is caused by the impact of solid particles. Erosion occurs in places which are not easily noticeable. This erosive wear phenomenon can be detected in the areas for instance boiler, pump impellers, rocket nozzles, turbine blades, pipe bends, helicopter engine, etc. [1,2,3,4] Research shows that wear phenomenon has a ruinous impact on the world energy expenditure which consumes 23% of the world's energy.[5] Furthermore, the expenditure owing to wear loss costs the industrialized nations an estimated 1-4% of their gross national product (GNP). Therefore, it is highly necessary to research in the area of wear resistant materials to acquire a suitable material.[6] The high chromium white cast irons (HCCI) are comprehensively utilized in the areas susceptible to wear in consideration to its remarkable wear resistance characteristics.[7] The HCCIs comes under ferrous alloys which retain 12-30 wt% chromium with carbon contents 1.6-3.6wt%.[8] The significance of the transition materials to enhance the wear resistance of cast irons have been analyzed by substantial number of studies. [9,10,11,12,13] The existing studies indicate that not only the stoichiometry is affected by the transition metals but also the hard carbide formation is immensely impacted. Which has considerable contribution to the wear behavior of cast irons. The aim of adding transition metals is to reform the eutectic carbides to increase the hardness, elevate hardenability of matrix and limit the pearlite development in the regions with these alloying elements between the eutectic carbides and the matrix.[14,15] The concentration of C in the matrix significantly affects the carbide volume fraction (CVF). Furthermore, higher C content results in an increase in the CVF, which in turn leads to improved hardness and wear resistance.[16] In as-cast form, these alloys consist of an austenitic matrix with M_7C_3 carbide as the main component.[17] This matrix can be transformed into martensite through heat treatment.[18] These alloys can exhibit high hardness and wear resistance when they contain a large amount of M_7C_3 eutectic carbides. A high concentration of C and Cr leads to a high volume of eutectic carbides, improving hardness and wear resistance, but reducing fracture toughness.[19] HCCIs solidify as primary austenite dendrites with a network of interdendritic eutectic carbides. During the destabilization heat treatment process, the austenite matrix is typically transformed into martensite.[20,21,22,23] Austenitic irons have hardness values between 500 and 520 HV and can be used in a few applications. However, heat-treated irons are necessary for a wider range of applications. Heat treatment at 1193-1333K for 1-6 hours (depending on the specific alloy composition), followed by air quenching at room temperature destabilize the austenite through precipitations of Cr-rich secondary carbides; This heat treatment is performed to increase the hardness of the material.[24] It is expected that the formation of MC carbides with excellent hardness and spherical morphology will improve the toughness of HCCI. In addition, primary MC carbides are typically formed at the beginning of solidification and are finely distributed throughout the iron matrix. The addition of Ti, Nb, and V can significantly promote the formation of MC primary carbides, as has been extensively studied by many researchers. Bedolla et al.[17,18,25] discovered that the addition of transition metal Nb and Ti to HCCI promotes to precipitation of NbC and TiC.V is an important transition metal to improve wear resistance however higher percentage of V is needed to get VC precipitation which eventually enhance the cost. Radulovic et al. found that the Fe-C-Cr-V alloy containing 3.28% V shows notable wear resistance.[26] Alvarez et al. studied that V does not seem to play a role as a grain refiner. [27] On the contrary, Xiaojun et al. found that the addition of TiC can improve the morphology of primary M_7C_3 carbides, and TiC precipitation significantly refines the final grain size without clustering in the matrix.[28] Although Ti is rapidly oxidized during melting and therefore special conditions for alloying are required when using an open induction furnace (not controlled atmosphere). The toughness of the matrix is also a key factor in determining wear resistance.[29] Methods such as semi-solid forming [30] and rare earth processing [31,32] have been utilized to enhance the toughness of HCCI by improving the size of the primary M_7C_3 carbides, though these methods have had narrow success. In erosion phenomenon the impact angle has a crucial role. Impact angle is one of the key and complicated factors to speculate the erosion lifetime. There are formulas such as cutting wear equation for erosion of oblique impact of square solid particles by Finnie [2] and to speculate the erosion as a consequence of vertical impact of spherical particles by Hutchings.[33] However, to speculate the erosion lifetime the above two equations are not precise always. Shimizu et al. studied the erosion rate of ferritic spherical-graphite cast iron (FDI) in different impact angles (0°,30°,60°,90°), and found that the erosion becomes maximum at impact angle about 60°.[34] Though several studies have been done on erosive wear or abrasive wear of HCCI to find the effect of transition metals, the papers focused on the combined effect of Ti and C content on erosive wear of HCCI are still inadequate. This paper thoroughly investigates the erosive wear behavior of HCCI with different Ti and C content.

Wear equation for erosion by Finnie:

$$Q = \frac{mV^2}{\mathcal{P}\psi K}\left(\sin 2\alpha - \frac{6}{K} Sin^2\alpha\right) \qquad \text{Eqn. 1}$$

Where Q is the volume of material, m is mass, V is the velocity, $\mathcal{P}$ is the flow stress, ψ is the depth of cut constant, K is the force constant, and α is the impact angle.

Erosion equation by Hutchings:

$$E = 0.003\frac{\alpha\rho\sigma^{1/2}v^3}{\epsilon_C{}^2 P^{3/2}} \qquad \text{Eqn. 2}$$

Where α is the indentation, ρ is the density of target material, σ is the density of eroded material, $\in_C$ is the strain, and P is the pressure.

Experimental Procedures

Materials Fabrication

HCCI with 27% Cr was employed as base metal for this study. C contents of 3, 3.5, 4 wt.% and Ti contents of 0, 1, and 2 wt.% were added to this base metal. The number of specimens were nine. The making of the specimens can be described concisely. 50 kg of raw materials were melted in a high induction furnace. The melted material was poured into a sand mold of 53 mm × 250 mm × 15 mm dimension. To cut the specimens in the dimension of 50 mm × 10 mm × 10 mm, a high-speed precision cutting machine (Refinetech Co., Ltd., RCA-234, Kanagawa, Japan) was employed. The accurate percentage of each alloy was measured utilizing the SPECTROLAB (AMETEK, Inc., Berwyn, PA, USA) and the results are shown in table 1. Scan electron microscopy integrated with energy dispersive X-ray spectroscopy (SEM+EDS) and X-ray diffraction were employed to analyze the microstructure before and after etching in 5% nitro-hydrochloric acid. ImageJ software was used to calculate the carbide volume fraction (CVF).[35]

Table 1. Chemical composition of the specimens (wt.%).

Test Material	C	Si	Mn	Cr	Ti	Fe
3C-0Ti	2.98	0.45	0.45	27.15	0.03	Bal.
3C-1Ti	2.97	0.47	0.43	27.09	1.06	Bal.
3C-2Ti	3.01	0.50	0.47	26.93	1.89	Bal.
3.5C-0Ti	3.35	0.46	0.45	27.29	0.07	Bal.
3.5C-1Ti	3.35	0.45	0.46	27.17	1.20	Bal.
3.5C-2Ti	3.32	0.48	0.44	27.03	2.07	Bal.
4C-0Ti	3.91	0.48	0.43	27.53	0.09	Bal.
4C-1Ti	3.82	0.53	0.40	27.19	1.30	Bal.
4C-2Ti	3.89	0.51	0.44	26.89	2.39	Bal.

Generally, HCCI is quenched after heating in the temperature range of 1173–1423 K, followed by tempering after heating at 693–813 K to alter the austenite to martensite and precipitate the secondary carbide.[16,24,36,37] Although, study by Purba et al. shows that high chromium based multi-component white cast iron shows the best erosive wear resistance with quenching only.[38] Several research papers show that the excellent wear resistance of the material is achieved due to higher hardness, however the toughness needs to be controlled in certain instances by refining a small portion of austenite in the microstructure after heat treatment.[35,39] That being so, materials with the highest hardness will be selected that may have marginal quantity of retained austenite (RA) in the microstructure after destabilization heat treatment within the favorable temperature range. As a result, the specimens in this study were heated in the temperature range of 1273–1323K. After the completion of the heating the specimens were cooled through air force cooling (AFC). X-ray diffraction (Ultima IV, Rigaku, Japan, with a Cu-K∝ source) was utilized to determine the phase of the microstructure of the material. To calculate the volume fraction of RA (f_{RA}) the following formula was applied.

$$f_{RA} = \frac{100\%}{1+G\left(\frac{I_{\propto}}{I_{\gamma}}\right)} \qquad \text{Eqn. 3}$$

where $I_{\propto}$ and I_{γ} are the peak intensities of $\propto$-Fe (200), (211) and γ-Fe (200), (220), (311), and G is the coefficient proportionate to the distinct composition as suggested in.[40]

Erosive Wear Test

In this current study, the selected specimens were eroded for 3600s utilizing uneven steel grit as the impact particles. In the time of erosion test 2Kg of uneven shaped steel grits (770 μm and 810 HV) was used as impact particles on each of the target specimen. To acquire accurate data the particle was exchanged with newer ones at every stage of erosion test. The nozzle pressure to inject the impact particles was 0.49 MPa at speed of 200m/s. The particles were injected in three different angles 30°,60°,and 90°. In addition, the erosive wear test was performed at room temperature. Figure 1 illustrates the schematic of the erosive wear test machine. The mass of each specimen was weighed before and after the test utilizing an automated scale (GH-300 produced by A&D Co. Ltd.) followed by the volumetric loss evaluation. The erosion rate was obtained by dividing the volumetric loss with the total erodent supplied. The probable erosive wear mechanism was identified by inspecting the erosion scratches of the worn surface as well as investigating the vertical section erodent surface.

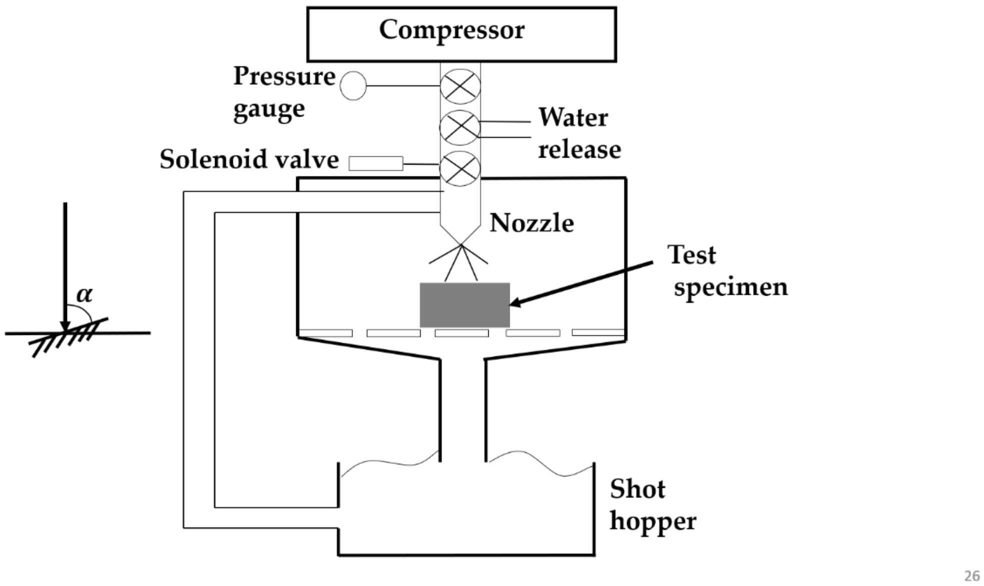

Figure 1. Schemetic of the erosive wear test machine.

Vickers Hardness Test

Each material was cut with dimensions of 10 mm × 10 mm × 10 mm and polished afterward. To calculate the micro-hardness and macro-hardness (applied load HV 0.1 Kgf and 30 Kgf, respectively) of the materials, Future-Tech Co., Ltd.: FV-800, Kanagawa, Japan Vickers hardness testers were utilized. The micro-hardness signifies the matrix hardness, and the macro-hardness signifies the hardness of the entire material (both matrix and carbide).Table 2 shows the macro hardness, matrix hardness, carbide fraction, and carbide size of all the specimens.

Table 2. Hardness, carbide fraction, and carbide size of the specimens.

Test Material	**3C-0Ti**	**3C-1Ti**	**3C-2Ti**
Macro hardness	870HV	815HV	768HV
Matrix hardness	643HV	558HV	524HV
Carbide fraction	41.2%	39.0%	39.2%
Carbide size	13.7μm	9.09μm	7.1μm
Test Material	**3.5C-0Ti**	**3.5C-1Ti**	**3.5C-2Ti**
Macro Hardness	916HV	863HV	792HV
Matrix hardness	665HV	612HV	549HV
Carbide fraction	42.3%	39.3%	39.1%
Carbide size	29.0μm	19.8μm	14.3μm
Test Material	**4C-0Ti**	**4C-1Ti**	**4C-2Ti**
Macro hardness	964HV	956HV	878HV
Matrix hardness	748HV	672HV	623HV
Carbide fraction	39.4%	41.0%	40.5%
Carbide size	39.8μm	32.5μm	26.7μm

Results and Discussion

Metallographic observation

The metallographic observation for materials for instance HCCI is one of the most essential factors in examining the wear properties of the material. That being the case, the test materials were separately etched in 5% nitro- hydrochloric acid for 6 min, with subsequent inspection using the scanning electron microscope. The microstructure of every specimen is displayed in Figure 2. It is shown by the images that a considerable number of carbides are precipitated in the microstructure. It is shown that regardless of the percentage of C or Ti, primary eutectic carbide M_7C_3 precipitates in all specimens. Earlier several studies [41,42,43,44] have been conducted to display the shape of the M_7C_3 carbide. It has been discovered that the M_7C_3 contains a hexagonal bravais lattice; although, an orthogonal crystal structure can be observed in special circumstance. TiC begins to emerge, with the addition of Ti. The precipitation of TiC has an evident impact on M_7C_3 carbide. The quantity of M_7C_3 carbides starts to decrease as a result of the growing percentage of Ti. The reason behind decreasing quantity of M_7C_3 carbide is the approach of Ti to precipitate in advance of M_7C_3; therefore, Ti absorbs C in the primary level. The inadequacy of C to produce M_7C_3 causes to the insufficiency of M_7C_3. The quantity of M_7C_3 begins to decrease with the precipitation of TiC, and the size of M_7C_3 carbide shrinks as well. Figure 3 (a) shows the microphotographs through optical microscopy (OM) after being etched in nital. It can be noticed that the microstructure consists of matrix with secondary carbides and eutectic carbides. Figure 3(b) shows that significant amount of $M_{23}C_6$ is precipitated along with TiC and Cr based M_7C_3.

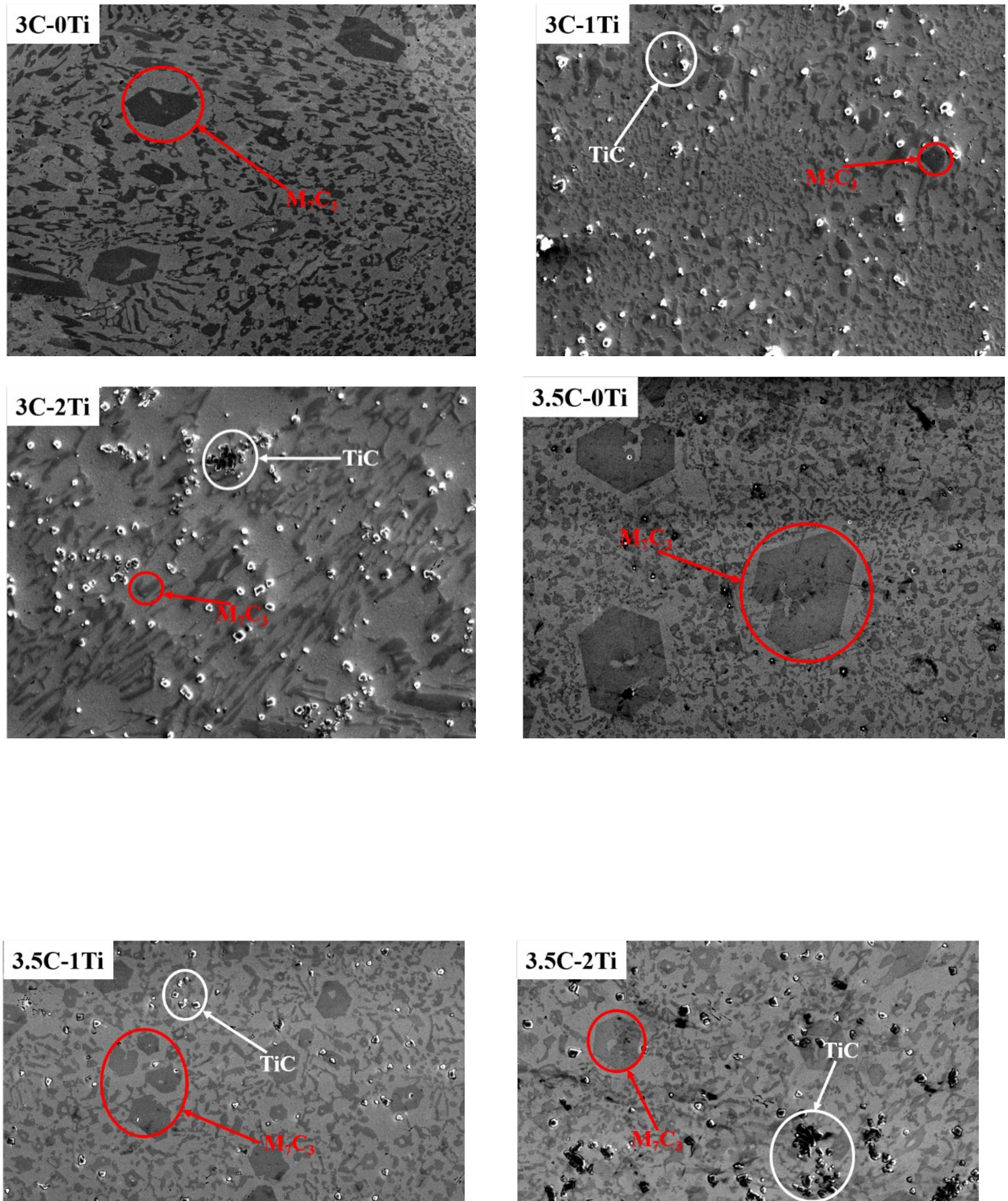

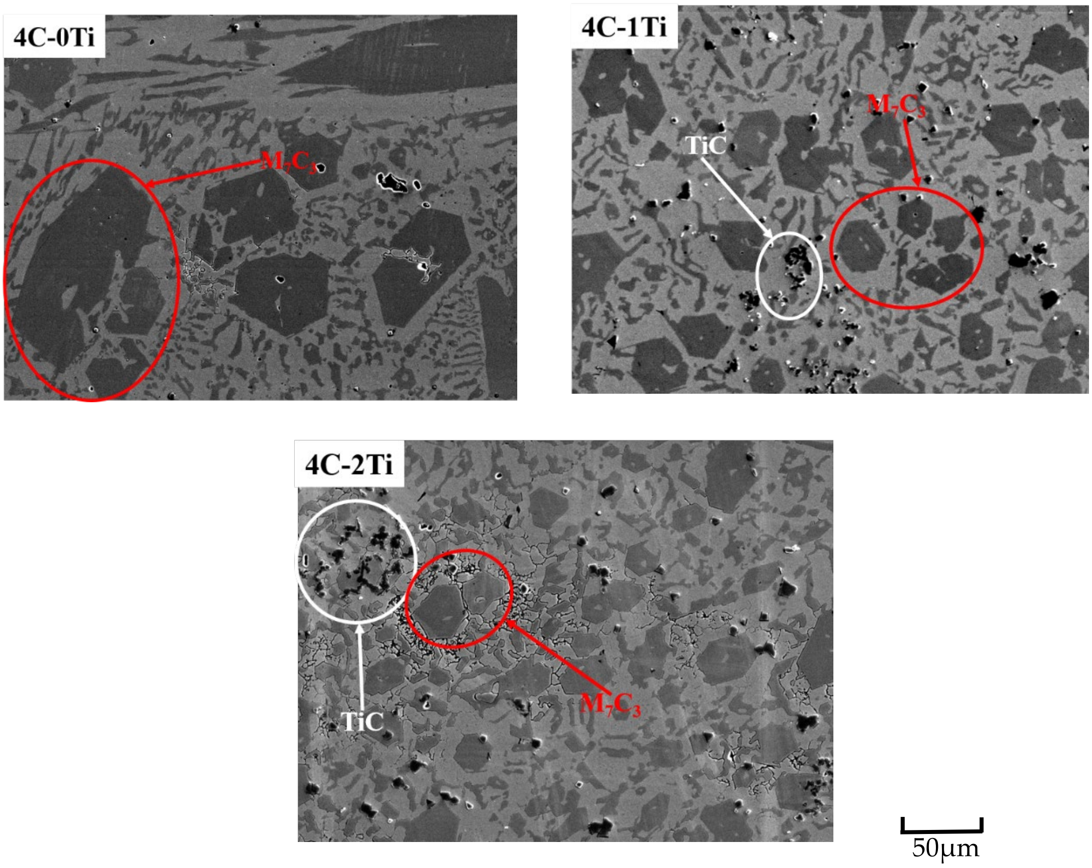

Figure 2. Microphotograph of matrix and carbide through SEM (red circles denote M_7C_3 carbides, and white circles denote TiC carbides).

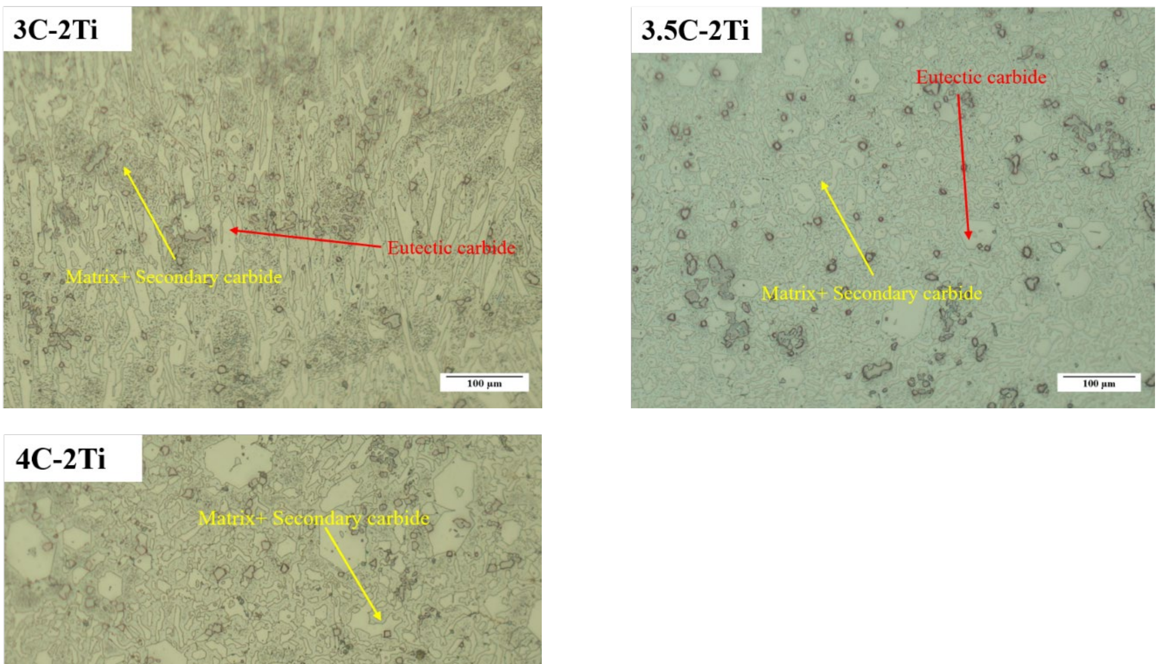

(a)

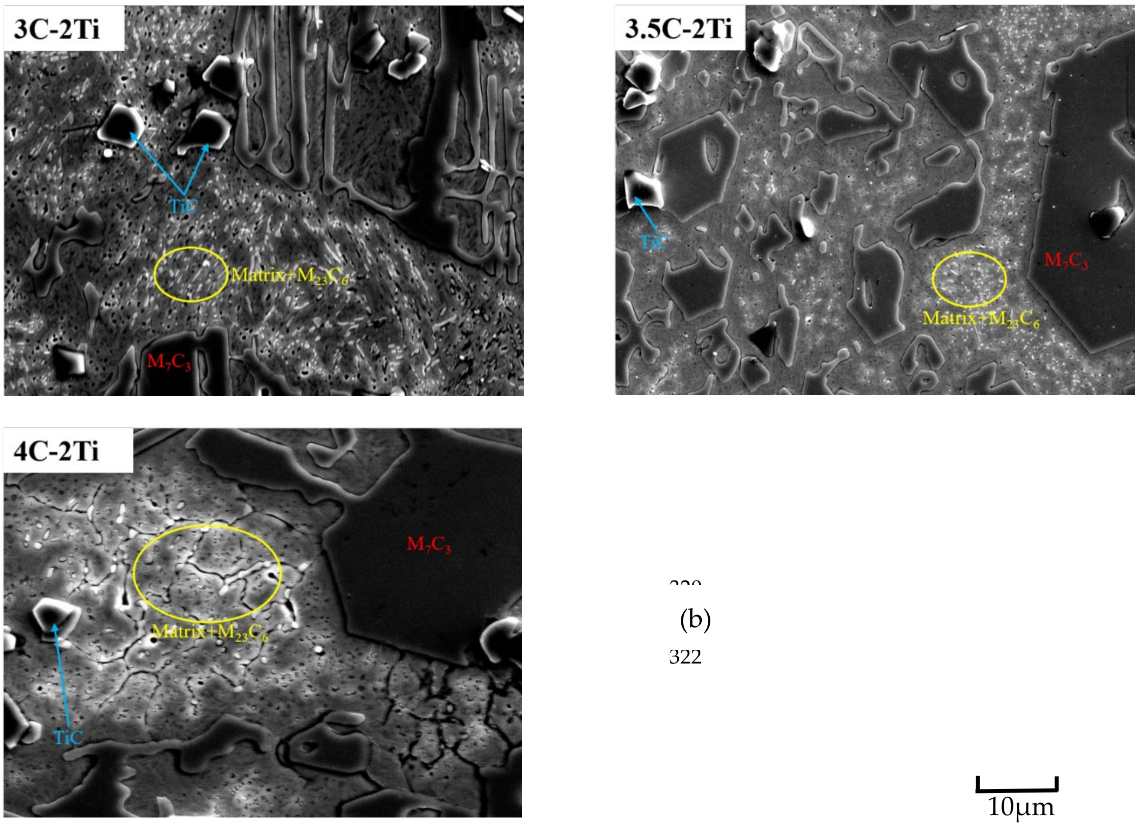

(b)

Figure 3. Secondary carbide obervation: (a) microphotographs using OM, (b) microphotographs using SEM.

The carbide size distribution is illustrated in Figure 4. It shows a descending tendency in the average particle size, with values 13.7, 9.09, and 7.1 μm for the Ti contents of 0, 1, and 2wt.%, correspondingly in the event of 3wt.% C. An identical trend is noticed for 3.5 and 4 wt.% C as well. The probable happening to shrink or refine M_7C_3 carbide is that whenever the Ti begins to absorb the C, the affability of the C content in the iron melt is low for chromium carbide, causing refinement of M_7C_3. A former research is in favorable agreement with this present study.[11] Although, a different incident is noticed when the test materials are supplemented with higher percentage of C. With an enrichment of the C content, the quantity of M_7C_3 carbides begins to grow.

The quantity of M_7C_3 begins to rise with a rise in the C content, and the size of the M_7C_3 carbides grows in addition. A tendency in the size enlargement of M_7C_3 is noticed. For the C content of 3 and 4wt.% the average particle size is 13.7 and 39.8 μm, correspondingly, in the event of 0wt.% Ti. A similar tendency is also noticed for 1 and 2 wt.% Ti specimens. A reasonable interpretation for this circumstance is the strong carbide forming trait of Cr. Greater percentage of C is consumed by greater amount of Cr which leads to dense M_7C_3 precipitation. Additionally, the C content in the stoichiometry sufficiently enhance the amount of M_7C_3. Figure 5 displays the X-ray diffraction (XRD) pattern of 3.5 wt.% C specimens. It is found that the matrix is mainly martensite and there is a negligible percentage of retained austinite. The mentioned three specimens 3.5C-0Ti, 3.5C-1Ti, and 3.5C-2Ti shows 10%, 3%, and 3.7% retained austenite (RA) respectively.

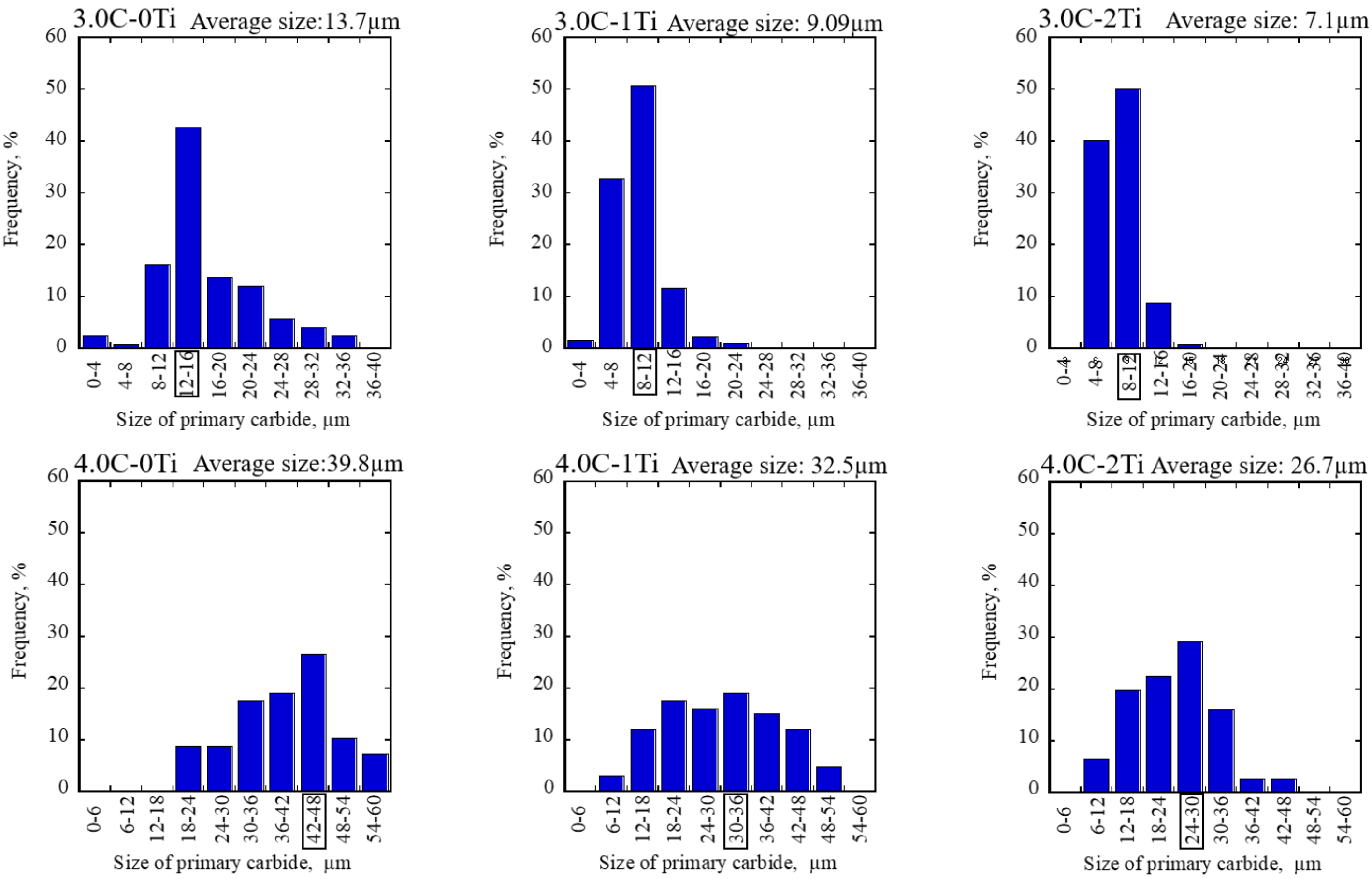

Figure 4. Carbide size distribution for the 3 wt.% C and 4 wt.% C specimens.

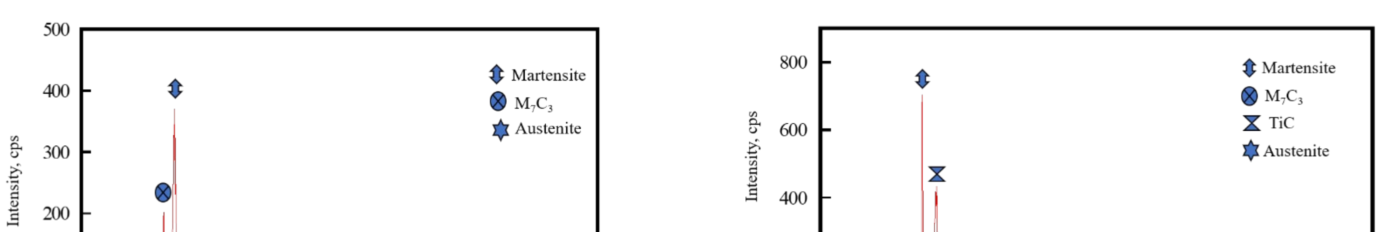

(a) (b)

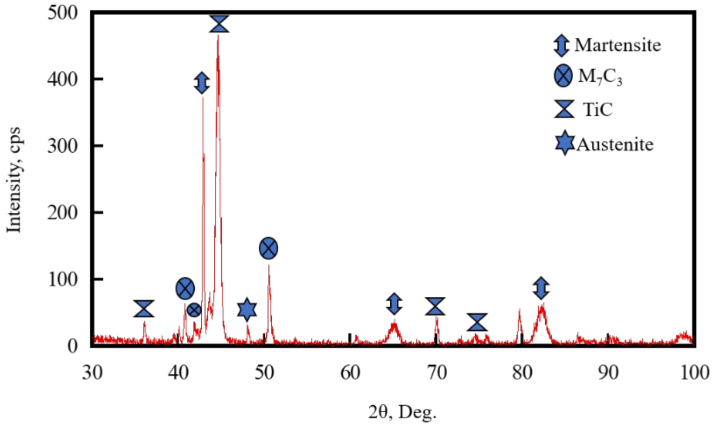

(C)

Figure 5. X-ray diffraction (XRD) patterns of the 3.5 wt.% C specimens: (a) 3.5C-0Ti, (b) 3.5C-1Ti, and (C) 3.5C-2Ti.

The carbide precipitation behavior of 27Cr seem to be densely distributed. The distribution of the added transition metal in the microstructure is difficult to locate. On that account, the 4 wt.% C test specimens with 0, 1, and 2 wt.% Ti were examined by EDS mapping. The results are displayed in Figure 6a-c. It can be identified from the microphotographs of the SEM-EDS images that the dark carbides are mostly occupied by Cr. A compact dispersion approach of M_7C_3 grows with the increase in C content. Although, the opposite tendency is observed with the rise in Ti content. The insufficiency of M_7C_3 is due to the advanced precipitation of TiC. The greater percentage of C and Ti contributes to the accumulation of TiC because of the superior affability of C.

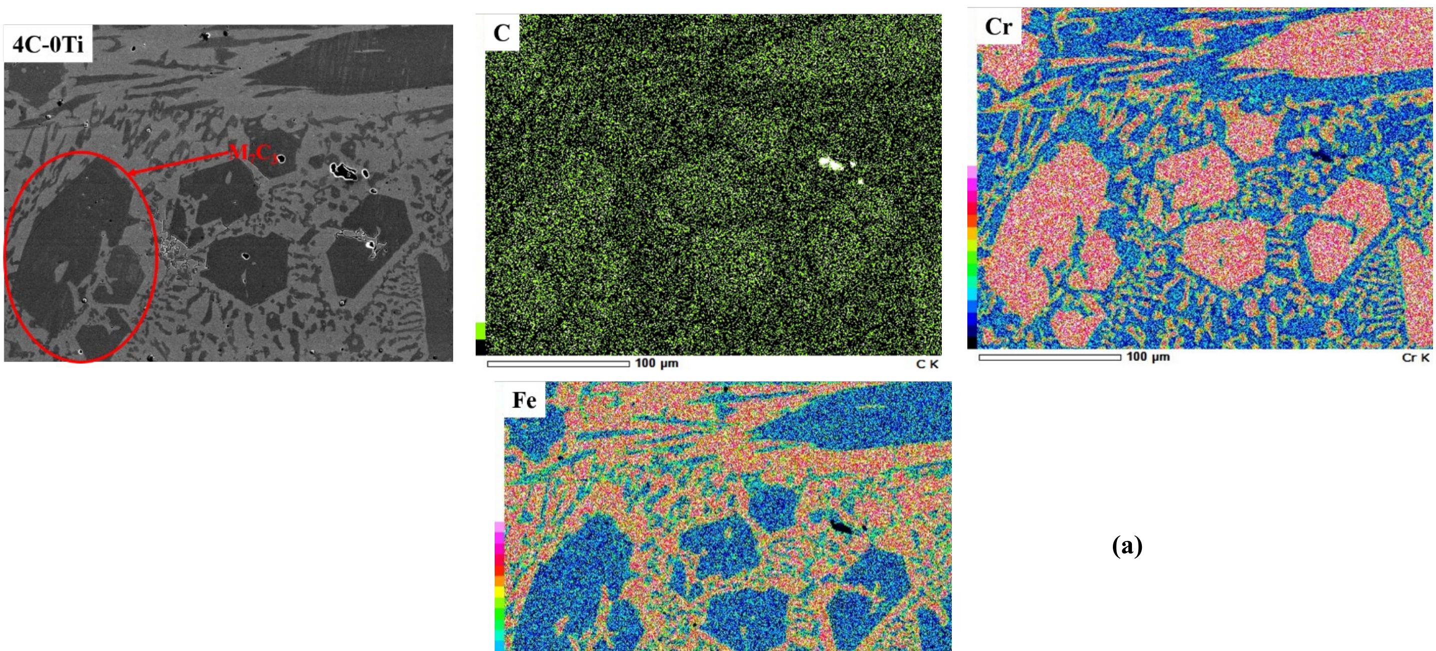

(a)

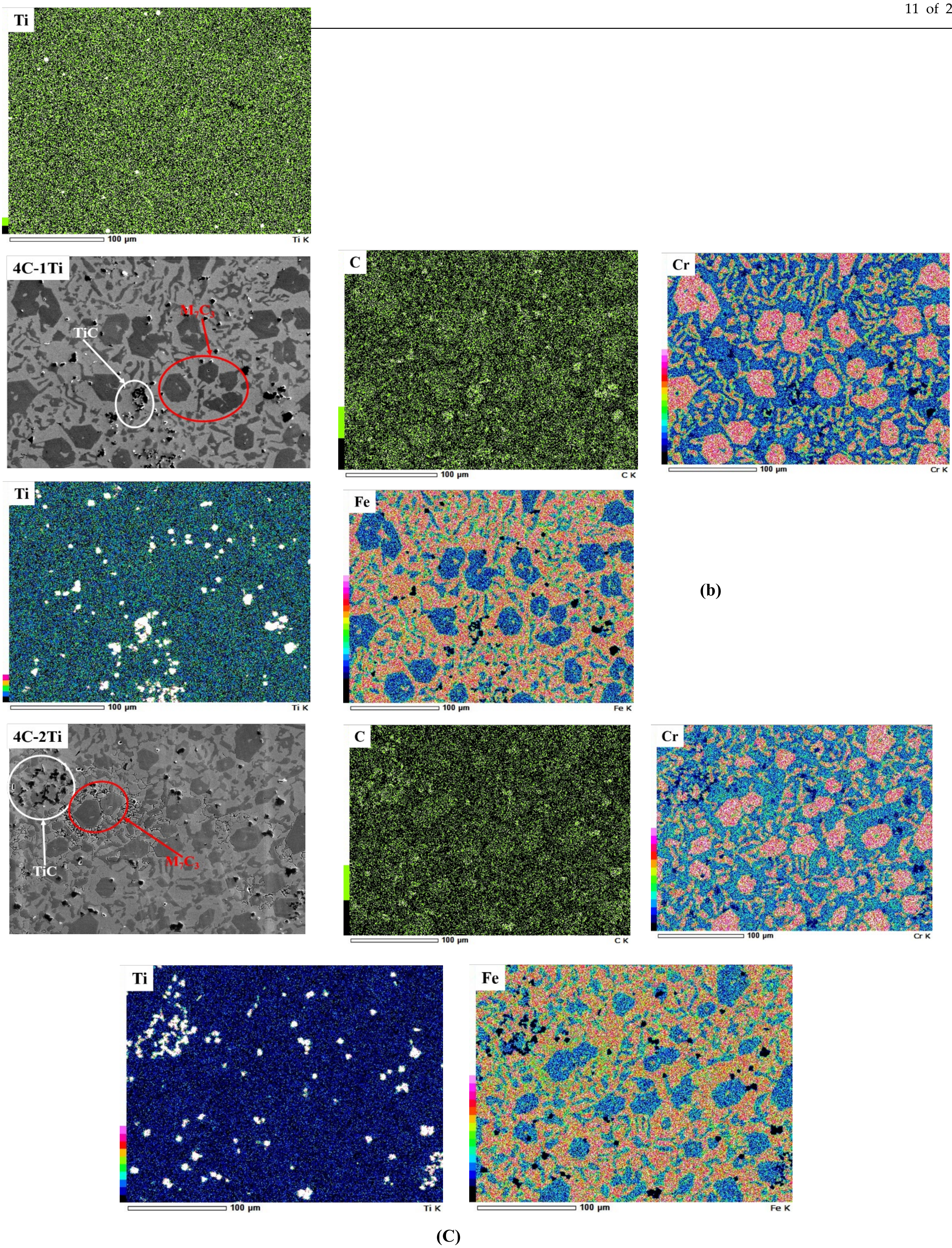

***Figure 6.** Distribution of chemical elements through SEM-EDS analysis of the 4 wt.% C specimen's wear surfaces: (a) 4C-0Ti specimen, (b) 4C-1Ti specimen, and (c) 4C-2Ti specimen.*

Erosive Wear Characteristics

This current study has been performed on 30°, 60°, 90° impact angle, as impact angle is one of the significant factors to determine the erosive wear. The importance of impact angle on erosive wear has been stated in several previous studies.[45,46] Figure 7 shows the erosion rate of each specimen in accordance with the impact angle. The X-axis indicates the impact angles, and the Y-axis indicates the amount of erosive wear loss. The results demonstrate that each of the test specimens experiences a similar wear loss tendency where the material loss intensifies at 60°impact angle. Compared to all the specimens, the 4C-0Ti demonstrated the lowest wear rate; although, with the increase in Ti content and the decrease in C content, the wear rate increase. The core reason behind the superior wear resistance achievement of 4C-0Ti is believed to be its superior hardness.

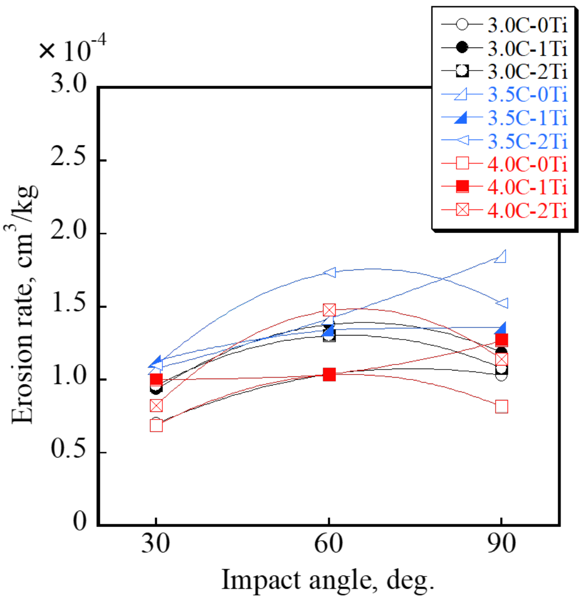

Figure 7. Relationship between erosion rate and impact angle.

Figure 8 displays relationship between the erosive wear rate and the hardness of every specimen. The square plot demonstrates the hardness, and the bar graph represents the wear rate. It is observed that the erosive wear rate declines as the hardness of every specimen rises. A significant role is played by the C content in affecting the Vickers hardness value. The specimens with 4 wt.% displayed the slightest wear rate in comparison with every C content. Although, the wear rate of the 4C specimens increased with increasing Ti content. The specimens with smaller C content and bigger Ti content directed to a lower Vickers hardness, which can be the cause of poor wear resistance. This finding is in good agreement with a former research.[47]

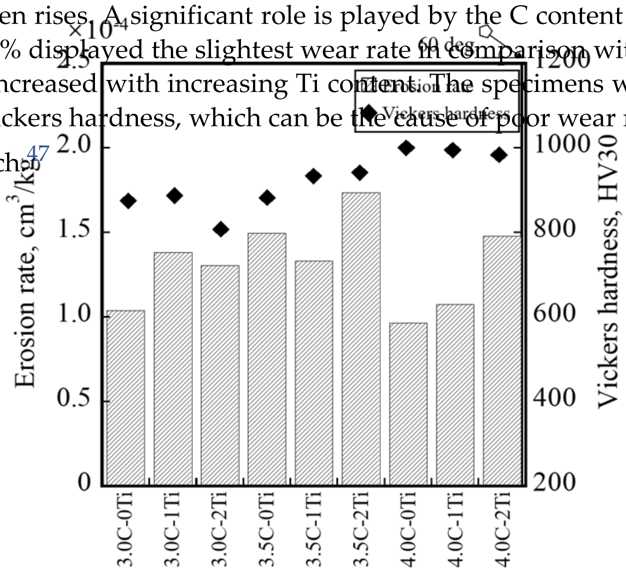

Figure 8. Relationship between erosion rate and Vickers hardness.

Figure 9 illustrates the relationship between the erosion rate and carbide average particle size. It exhibits a correlation which is, the erosion rate increases as the carbide average particle size decreases. It can be predicted that the bigger sized carbides notably withstand the impact particle during erosion test hence demonstrates lowest wear resistance.

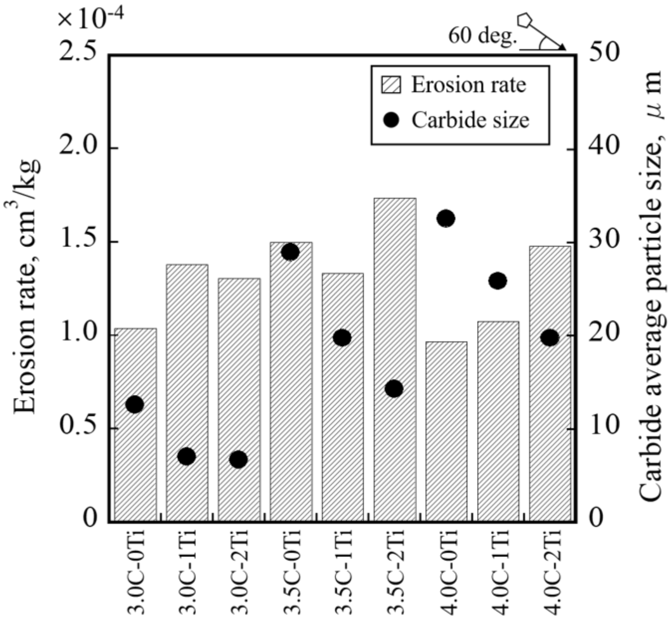

Figure 9. Relationship between erosion rate and carbide size.

Figure 10 illustrates the impact of carbide fraction on the erosion rate. The carbide fraction is affected by the Ti additions. For any given C content, C produces more Cr (M_7C_3) carbides than Ti (MC) carbides. Therefore, at any given C content, the amount of carbide is reduced when Ti is added. In addition, the degree of eutectic saturation of the structure decreases as Ti is added. Since Ti carbides form at higher temperatures during solidification, the C content of the remaining liquid metal will be decreased, as will the degree of eutectic saturation. Furthermore, the C contents of these alloys range from 3 – 4%, so the base irons in each C series are all hypereutectic alloys and contain primary M_7C_3 carbides. With the addition of Ti, the amount of primary M_7C_3 carbide is reduced. Densely distributed hard carbides strongly resist the thrust of the impact particles to reduce wear.

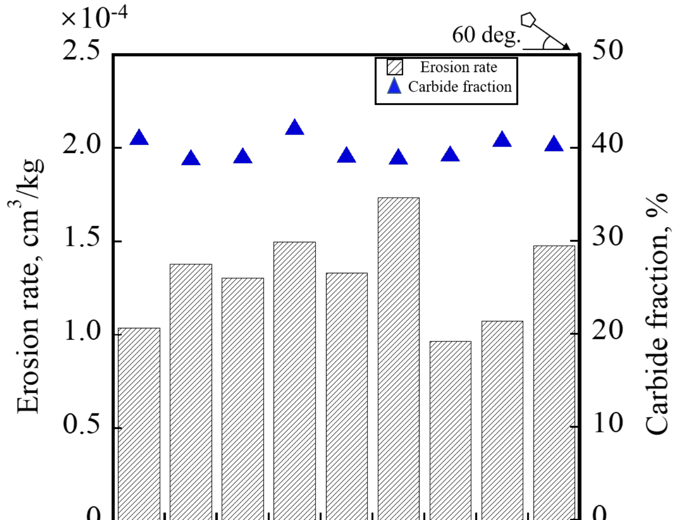

Figure 10. Relationship between erosion rate and carbide fraction.

Figure 11 shows the hardness of the specimens before and after the erosion test. The hardness of the matrix before and after erosion test is shown as well. According to the previous research, it can be said that the erosion might be affected by the work hardening that occurs on the worn surface after the test. This present study shows that the work hardening has occurred on the surface of all the specimens due to the impact of particles. The hardness of the 3C specimen is increased by about 10% after the erosion test, however it is lower than that of the 4C specimen. In addition, because of the increase in C content the strengthening of the matrix was confirmed hence the hardness of the matrix is increased.

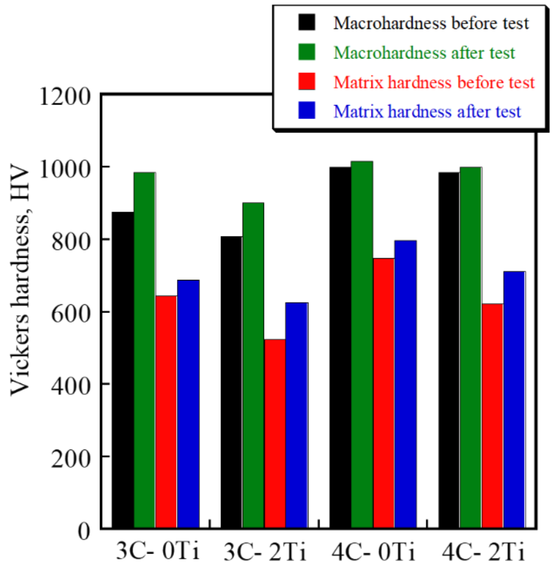

Figure 11. Hardness of the specimens before and after the erosion test.

Eroded Surface Observation

Eroded surface observation is significant for analyzing the erosive wear behavior. In order to confirm the cause of the erosive wear phenomenon the eroded surface and wear depth observation is performed in 3D laser microscope. The 3.5C and 4C specimens exhibit the similar result, due to that the 3.5C specimens are excluded. 3C-0Ti, 3C-2Ti, 4C-0Ti , and 4C-2Ti are used for explanation. It is illustrated by the Figure 12 that there are no considerable differences between the specimens wear depth values. The average wear depth was about 22 μm.

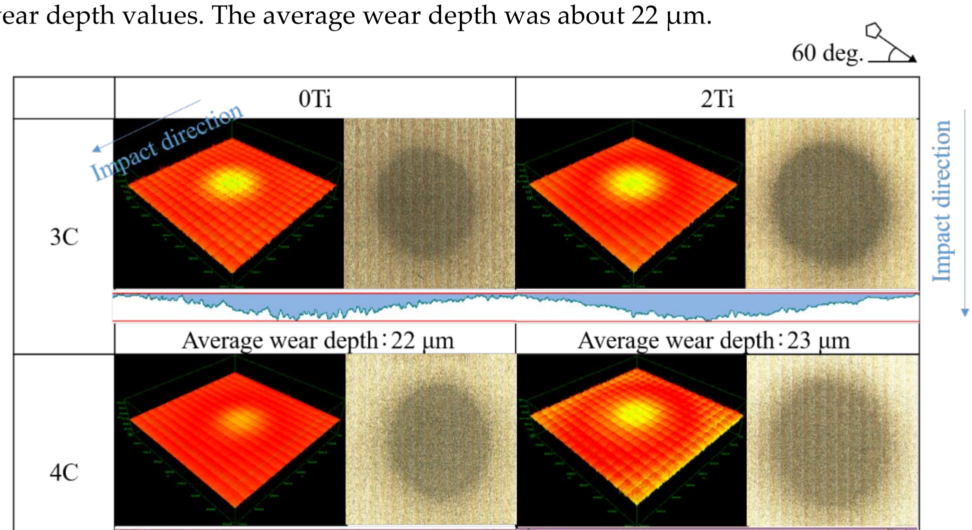

Figure 12. Eroded surface observation in 3D laser microscope..

Since no significant difference in erosive wear depth is observed with 3D laser microscope, the eroded surface is examined by the SEM. Figure 13 shows that the influence of Ti is absent. The microcutting is noticed in all the specimens is denoted with yellow circles. Figure 14 shows the roughness and cracking condition of the mentioned specimens. Lower C specimen 3C shows no crack with a comparatively smoother surface condition. However, higher C specimen 4C exhibits cracks and the condition of the surface is rougher than 3C specimens.

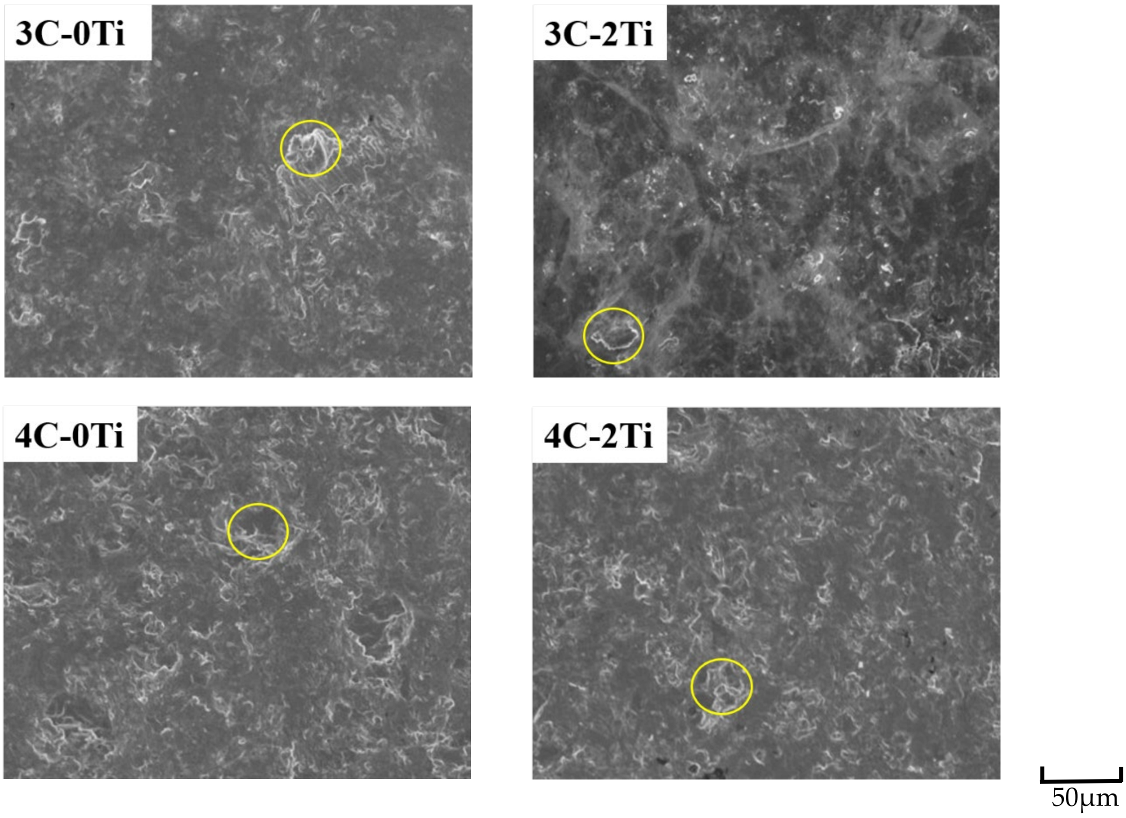

Figure 13. Eroded surface observation in scan electron microscope (SEM).

3C-0Ti
3C-2Ti
4C-0Ti

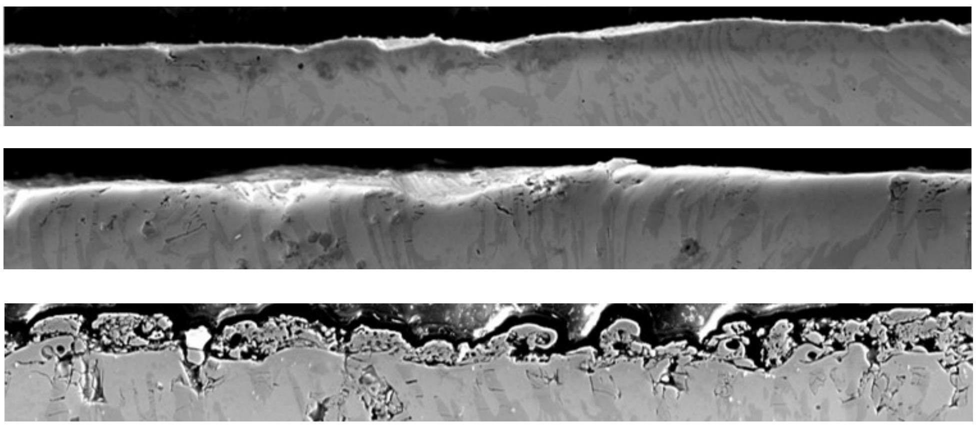

4C-2Ti

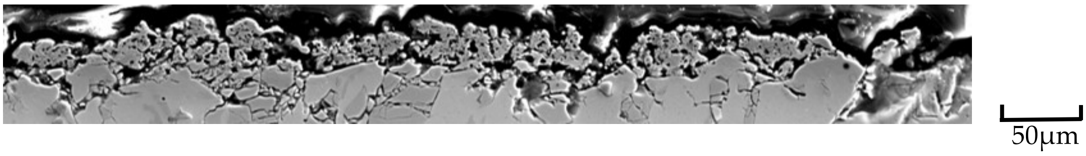

Figure 14. ***Roughness and cracking condition of the specimens.***

In order to determine the cause of the difference in microcutting and roughness it is essential to explain the effect of carbide particle size on the wear mechanism. Therefore, the eroded surface cross section was observed. The erosive wear mechanism of the fine carbides in the 3C-0Ti and 3C-2Ti specimens are explained firstly in the Figure 15.

It can be noticed that the matrix experience plastic deformation and cracks are found in the fine M_7C_3 carbide. In addition, it is confirmed that the plastic deformation layer of the 2Ti specimen was thicker than that of the 0Ti specimen. From these facts, it is considered that the erosive wear resistance starts to decrease because of the refinement of carbide. As a result, it cannot withstand the deformation. With the time the impact particles bring more cracked carbides and the matrix is scraped off with it.

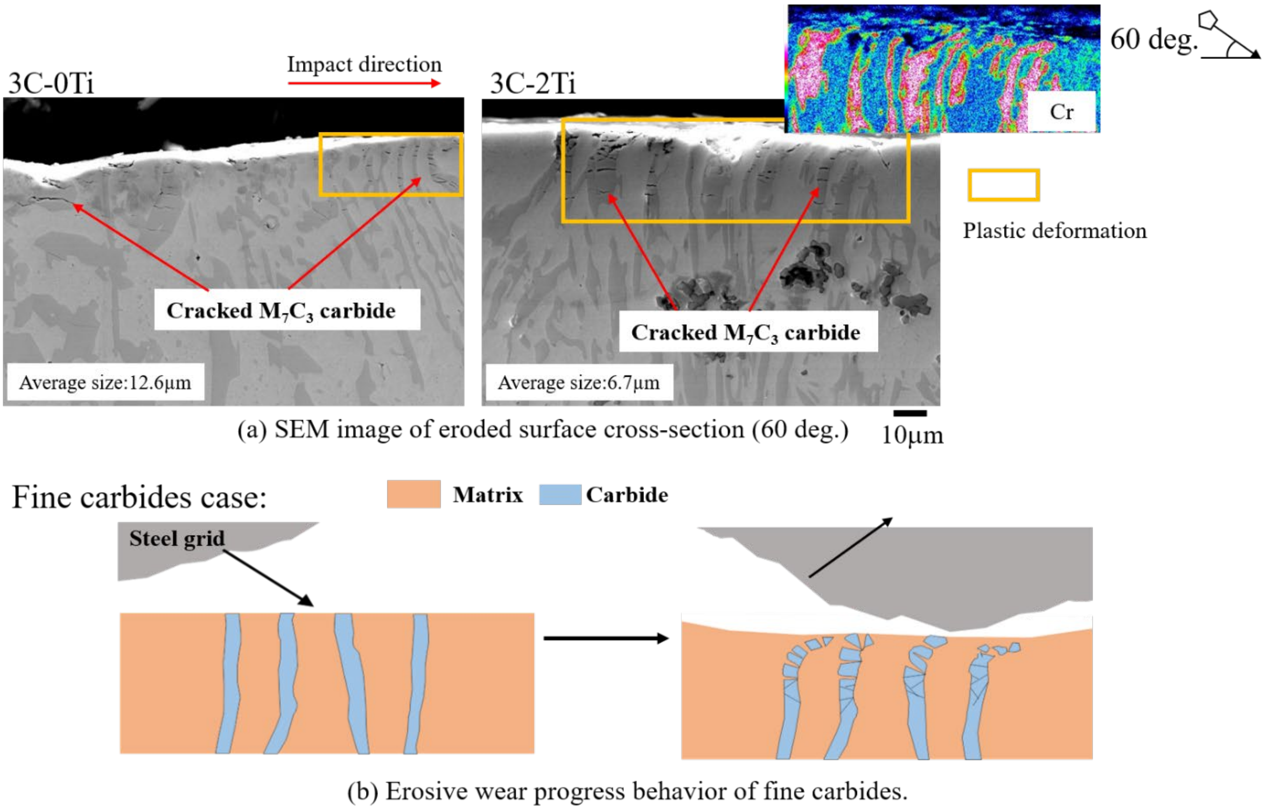

Figure 15. Erosive wear mechanism of the fine carbides in the 3C-0Ti and 3C-2Ti specimens: (a) SEM image of the eroded surface cross-section, (b) Erosive wear progress behavior of fine carbides.

However, a reverse scenario is observed for the 4C specimens. Figure 16 displays the wear mechanism of 4C specimens with coarse carbides. It is noticed that the plastic deformation and coarse carbide cracks are present in all materials. It can be considered that the increase in the wear resistance is due to the strengthening of the matrix and the coarsening of carbides due to the increase in the C content.

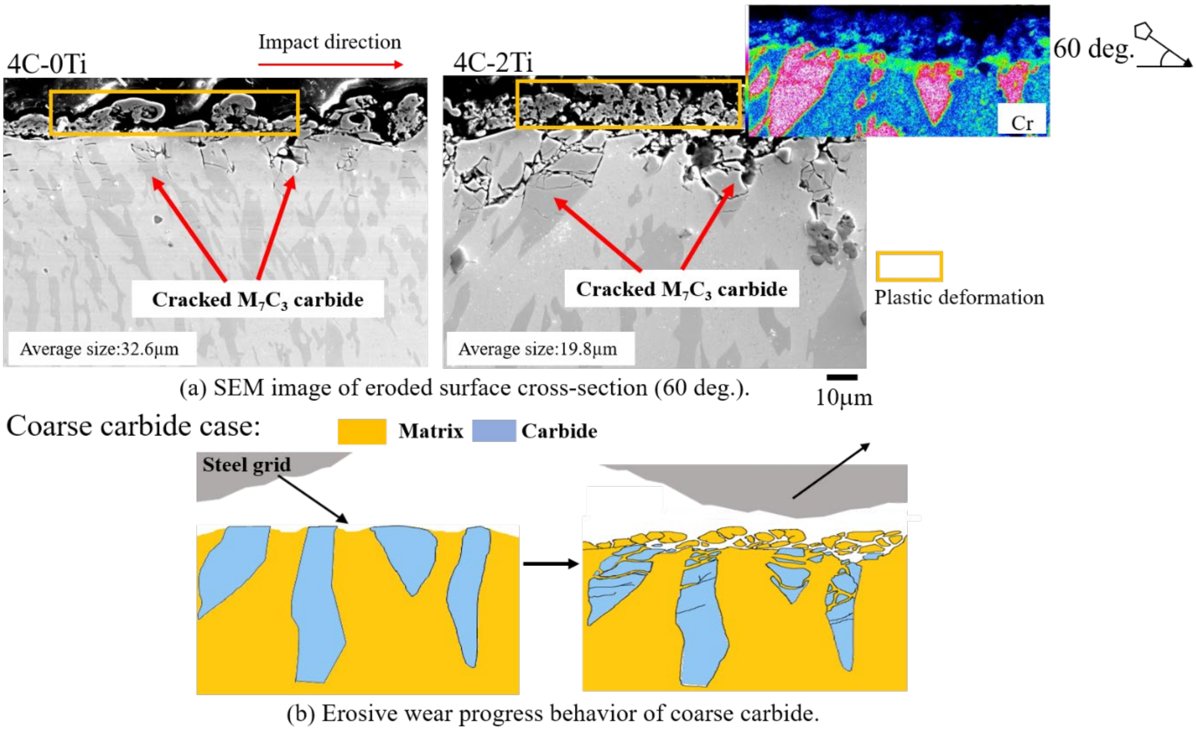

Figure 16. Erosive wear mechanism of the coarse carbides in the 4C-0Ti and 4C-2Ti specimens: (a) SEM image of the eroded surface cross-section, (b) Erosive wear progress behavior of coarse carbides.

Conclusion

After the investigation on the effects of Ti and C on the erosive wear behaviour of HCCI the below conclusions can be summarized:

1. The addition of Ti to HCCI prompts the M_7C_3 carbides in the microstructure to become finer. With the increase in Ti for all specimens more TiC precipitates that results to reduction in carbide fraction and size.

2. The carbide size and fraction have significant impact on the erosive wear. Decrease in carbide size and carbide fraction results to lower hardness and makes the specimen easy target for impact particle to erosion.

3.By increasing the C content to HCCI more M_7C_3 starts to precipitate in bigger size. A correlation is found between erosion rate and M_7C_3 carbide size, which is the erosion rate increased as the average particle size of M_7C_3 carbides become finer as a result of more Ti addition.

5. A material composition with highest C and lower Ti content generally demonstrates the best erosive wear resistance due to bigger carbide size, carbide fraction and higher hardness.

Author Contributions: Writing-Original draft preparation, Conceptualization, Investigation, Reviewing and Editing, M.J.H., Methodology, Resources, Supervision, K.S., Formal analysis, Writing-Review and Editing, K.K., Project administration, R.H.P. and Y.G. All authors have read and agreed to the published version of the manuscript.

Funding: There is no external funding for this research.

Data Availability Statement: The data presented in this study are available on request from the corresponding author.

Conflicts of Interest: The authors declare no conflict of interest.

Acknowledgment: This paper is an invited submission to IJMC selected from presentations at the 74th World Foundry Congress, held October 16 to 20, 2022, in Busan, Korea, and has been expanded from the original presentation.

References

1. Antonov Maksim, Veinthal Renno, Huttunen-Saarivirta Elina, Hussainova Irina, Vallikivi Ahto, Lelis Martynas, Priss Jelena. Effect of oxidation on erosive wear behavior of boiler steels. Tribol Int 2013;68:35–44.
2. Finnie I. Erosion of surface by solid particles. Wear 1960;3:87–103.
3. Wood Robert JK. Friction, lubrication, and wear technology. In: ASM handbook, vol. 18. United States of America; 2017. p. 266–89.
4. Archard JF. Contact and rubbing of flat surface. J Appl Phys 1953;24(24):981–8.
5. K. Holmberg and A. Erdemir: Friction, 5 (2017), 263.
6. Mang, T.; Bobzin, K.; Bartels, T. *Industrial Tribology: Tribosystems, Friction, Wear and Surface Engineering, Lubrication*; WileyVCH: Weinheim, Germany, 2011; p. 1.
7. Gahr, K.H.Z.; Scholz, W.G. Fracture Toughness of White Cast Irons. *JOM* 1980, *32*, 38–44.
8. Francisco Vapeani Guerra, C.P.; Tabrett, I.R.; Sare, M.R. Ghomashchi, Microstructure property relationships in high chromium white iron alloys. *Int. Mater. Rev.* 1996, *41*, 59.
9. Y.Z. Lv, Y.F. Sun, J.Y. Zhao, G.W. Yu, J.J. Shen, S.M. Hu, Effect of tungsten on microstructure and properties of high chromium cast iron, Mater. Des. 39 (2012) 303–308.
10. E. Cortés-Carrillo, A. Bedolla-Jacuinde, I. Mejía, C.M. Zepeda, J. Zuno-Silva, F.V. Guerra-Lopez, Effects of tungsten on the microstructure and on the abrasive wear behavior of a high-chromium white iron, Wear 376–377 (2017) 77–85.
11. M. Filipovic, Z. Kamberovic, M. Korac, M. Gavrilovski, Microstructure and mechanical properties of Fe–Cr–C–Nb white cast irons, Mater. Des. 47 (2013) 41–48.

12. Y. Zhang, Y.F. Sun, S. Guan, X. Deng, X.Y. Yan, Effect of titanium and tungsten on the structure and properties of heat-abrasion resistant steel, Mater. Sci. Eng., A 478 (2008) 214–220.
13. Wang, H.; Yu, S.F.; Khan, A.R.; Huang, A.G. Effects of Vanadium on Microstructure and Wear Resistance of High Chromium Cast Iron Hardfacing Layer by Electroslag Surfacing. *Metals* 2018, *8*, 458. https://doi.org/10.3390/met8060458
14. Ono, Y.; Murai, M.; Ogi, K. Partition Coefficients of Alloying Elements to Primary Austenite and Eutectic Phases of Chromium Irons of Rolls. *ISIJ Int.* 1992, *32*, 1150.
15. Laird, G. Microstructures of Ni-Hard I, Ni-Hard IV, and High Cr White Cast Irons. *AFS Trans.* 1991, *99*, 339.
16. Todaka, T.; Shimizu, K.; Kusumoto, K.; Purba, R.H.; Gaqi, Y. Effect of Carbon Content on Three-body Abrasive Wear Characteristics of 28Cr-3Ni Cast Alloys. *ISIJ Int.* 2021, *61*, 2274–2283.
17. Bedolla-Jacuinde, A.; Correa, R.; Quezada, J.G.; Maldonado, C. Effect of titanium on the as-cast microstructure of a 16%chromium white iron. *Mater. Sci. Eng. A* 2005, *398*, 297.
18. Bedolla-Jacuinde, A.; Guerra, F.V.; Mejía, I.; Zuno-Silva, J.; Rainforth, M. Abrasive wear of V-Nb-Ti alloyed high-chromium white irons. *Wear* 2015, *332–333*, 1006.
19. Gahr, K.-H.Z.; Doane, D.V. Optimizing fracture toughness and abrasion resistance in white cast irons. *Met. Mater. Trans. A* 1980, *11*, 613.
20. Pearce, J.T.H. Examination of M7C3 carbides in high chromium cast irons using thin foil transmission electron microscopy. *J. Mater. Sci. Lett.* 1983, *2*, 428–432.
21. Peev, K.; Radulovic, M.; Fiset, M. Modification of FeCr-C alloys using mischmetal. *J. Mater. Sci. Lett.* 1994, *13*, 112–114.
22. Kibble, K.A.; Pearce, J.T.H. An examination of the effects of annealing heat treatment on secondary carbide formation in 25%Cr high chromium irons. *Cast Met.* 1995, *8*, 123–127.
23. Powell, G.L.F.; Laird, G., II. Structure, nucleation, growth and morphology of secondary carbides in high chromium and Cr-Ni white cast irons. *J. Mater. Sci.* 1992, *27*, 29–35.
24. Powell, G. Improved wear-resistant high-alloyed white irons-A historical perspective. In Proceedings of the International Congress on Abrasion Wear Resistance Alloyed White Cast Iron for Rolling and Pulverizing Mills, Fukuoka, Japan, 16–20 August 2002.
25. Bedolla-Jacuinde, A. Microstructure of vanadium-, niobium and titanium-alloyed high-chromium white cast irons. *Int. J. Cast Met. Res.* 2001, *13*, 343.
26. Radulovic, M. Fiset, K. Peev, M. Tomovic, The influence of vanadium on fracture toughness and abrasion resistance in high chromium white cast irons, J. Mater. Sci. 29 (1994) 5085–5094.)
27. W. Solano-Alvarez, L. Fernandez Gonzalez, H.K.D.H. Bhadeshia,The effect of vanadium alloying on the wear resistance of pearlitic rails,Wear, Volumes 436–437,2019.
28. Wu, X.; Xing, J.; Fu, H.; Zhi, X. Effect of titanium on the morphology of primary M7C3 carbides in hypereutectic high chromium white iron. *Mater. Sci. Eng. A* 2007, *457*, 180–185.
29. Dogan, O.N.; Hawk, J.A.; Laird, G., II. *Metall. Mater. Trans. A* 1997, *28A*, 1315–1327.
30. Huang, Z.F.; Huang, W.D.; Zhang, A.F.; Xing, J.D. *J. Xi'an Jiaotong Univ.* 2005, *39*, 775–778.
31. Llewellyn, R.J.; Yick, S.K.; Dolmanb, K.F. *Wear* 2004, *256*, 592–599.
32. Qin, Z.R.; Nie, L.W. *Chin. Pet. Mach.* 1998, *26*, 20–23.
33. I.M. Hutchings, A model for the erosion of metals by spherical particles at normal incidence, Wear 70 (1981) 269–281.
34. K. shimizu, T. Noguchi, H. Seitoh, M. Okada, Y. Matsubara, FEM analysis of erosive wear,Wear,Volume 250,Issues 1-12,2001,Pages 779-784.
35. Schneider, C., Rasband, W. & Eliceiri, K. NIH Image to ImageJ: 25 years of image analysis. *Nat Methods* 9, 671–675 (2012). https://doi.org/10.1038/nmeth.2089.(5 September 2022).
36. Karantzalis, A.E.; Lakatou, A.; Diavati, E. Effect of Destabilization Heat Treatments on the Microstructure of High Chromium Cast Iron: A Microscopy Examination Approach. *J. Mater. Eng. Perform.* 2009, *18*, 1078–1085.
37. Kishore, K.; Kumar, U.; Dinesh, N.; Adhikary, M. Effect of Soaking Temperature on Carbide Precipitation, Hardness, and Wear Resistance of High-Chromium White Cast Iron. *J. Fail. Anal. Prev.* 2020, *20*, 249–260.
38. Purba, R.H.; Shimizu, K.; Kusumoto, K.; Todaka, T.; Shirai, M.; Hara, H.; Ito, J. Erosive Wear Characteristics of High-Chromium Based Multi-Component White Cast Irons. *Tribol. Int.* 2021, *159*, 106982.
39. Yu, S.K.; Sasaguri, N.; Matsubara, Y. Effects of Retained Austenite on Abrasion Wear Resistance and Hardness of Hypoeutectic High Cr White Cast Iron. *Int. J. Cast Met. Res.* 1999, *11*, 561–566.
40. Sun, J.; Hao, Y. Microstructure Development and Mechanical Properties of Quenching and Partitioning (Q&P) Steel and an Incorporation of Hot-Dipping Galvanization during Q&P Process. *Mater. Sci. Eng. A.* 2013, *586*, 100–107.

41. Ma, S.; Xing, J.; He, Y.; Li, Y.; Huang, Z.; Liu, G.; Geng, Q. Microstructure and Crystallography of M7C3 Carbide in High Chromium Cast Iron. *Mater. Chem. Phys.* 2015, *161*, 65–73.
42. Liu, S.; Zhou, Y.; Xing, X.; Wang, J.; Yang, Y.; Yang, Q. Agglomeration Model of (Fe, Cr)7C3 Carbide in Hypereutectic FeCr-C Alloy. *Mater. Lett.* 2016, *183*, 272–276.
43. Geng, B.; Li, Y.; Zhou, R.; Wang, Q.; Jiang, Y. Formation Mechanism of Stacting Faults and its Effect on Hardness in M7C3 Carbides. *Mater. Charact.* 2020, *170*, 110691.
44. Laird, G.; Gundlach, R.; Rohrig, K. *Abrasion-Resistant Cast Iron Handbook*; AFS: Oakland, CA, USA, 2000.
45. Lei Xiao, Kazumichi Shimizu, Kenta Kusumoto, Impact Angle Dependence of Erosive Wear for Spheroidal Carbide Cast Iron, MATERIALS TRANSCATIONS, 2017, Volume 58, Issue 7, Pages 1032-1037.
46. D. Tabor, The Hardness of Metals, Charendon Press, Oxford, 1951, pp. 115-140.
47. Banadkouki, S.S.G.; Mehranfar, S. Wear Behavior of a Modified Low Alloy as Cast Hardening White Iron. *ISIJ Int.* 2012, *52*, 2096–2099.